Progress In Electromagnetics Research B, Vol. 37, 143–169, 2012

APPLICATION OF A HYBRID MODEL FOR THE SUSCEPTIBILITY OF COMPLEX FORM METALLIC WIRES PERTURBED BY EM NEAR-FIELD RADIATED BY ELECTRONIC STRUCTURES

E. R. Rajkumar, B. Ravelo*, M. Bensetti, and P. Fernandez-Lopez

IRSEEM, EA 4353, Graduate School of Engineering ESIGELEC, Technopole du Madrillet, Av. Galilée, BP 10024, 76801 Saint Etienne du Rouvray Cedex, France

Abstract—A modeling of the metallic wires susceptibility facing to the disturbances caused by electromagnetic (EM) near-field (NF) radiated by electronic structures in radio frequencies (RF) is introduced by using a hybrid method. This latter is based on the use of the given EM-data calculated or determined from the standard computation tools associated with basic analytical methods expressing the coupling voltages at the victim wire extremities and the EM-NF radiations. In difference to the classical methods based on the far-field radiations, the main benefit of this method lies on the possibility to take into account the evanescent waves from the disturbing elements. The basic principle illustrating the hybrid method principle is explained. To verify the relevance of the method proposed, we consider a metallic wire having cm-length above the ground plane disturbed by the EM-near-waves from the electronic circuits in proximity. For that, we model the EM radiation of the disturbing electronic circuits and then, apply the hybrid method to evaluate the coupling voltages induced through the wires. By considering the radiations around hundreds MHz, we demonstrate that the hybrid method proposed enables us to generate voltages in good agreement with the simulations performed with the commercial tools. Two types of realistic configurations are studied. First, with a microstrip loop circuit radiating at about 0.7 GHz, we calculated induced voltages at the extremities of the structures. Then, the same analysis was made with a 3D-model coil self for the large band from 0.1 GHz to 0.5 GHz. The results are in good accordance between the terminal voltages of

Received 9 November 2011, Accepted 4 December 2011, Scheduled 13 December 2011

* Corresponding author: Blaise Ravelo (blaise.ravelo@yahoo.fr).

the wire. The relative error in the second configuration falls less than 10%. This investigation is important for the EM compatibility (EMC) analysis of the radiating coupling between wires and complex electrical and electronic systems disturbed by RF harmonics.

1. INTRODUCTION

With the increase of the integration density of the modern electrical and electronic systems, the analysis of electromagnetic interference (EMI) and electromagnetic compatibility (EMC) issues become one of the primary importance and unavoidable step during the design process [1–7]. This effect can be found in various stages of the different chains for example in the automotive vehicles or aeronautic engines [8–12]. In fact, the main problems of EMC occur naturally when integrating power electronic and RF/microelectronic circuits operating in different frequency ranges. This incompliance is much more obvious in presence of the system including electronic devices and metallic wires. Till now, most of the EMC studies made in this context are performed with the consideration of the conducting harmonic disturbances, for example, caused by DC/DC or DC/AC converters [13–15]. Fig. 1 illustrates the different steps usually considered for evaluating the electrical parameters linked to the susceptibility effects.

Nevertheless, with the feature size reduction, the EM couplings based on the wave's radiation are as much as significant and can also generate unintentional disturbances.

To study such a radiation, the IRSEEM laboratory developed a near-field (NF) test bench [16–18] and also an inverse-method modeling method based on the optimization of equivalent sources constituted by EM elementary dipoles capable to reproduce the same radiation as the disturbing elements [19–24]. Fig. 2 explains the global methodology of the radiation modeling developed at IRSEEM [19]. But only the radiated emission modeling is not enough for investigating the EMC coupling in electronic systems.

We need also precise knowledge on the immunity of the systems facing to the EM radiated aggressions [25–27]. This is why in this

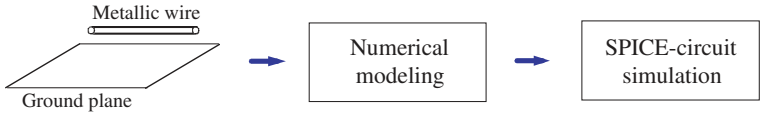

Figure 1. Different steps of susceptibility modeling.

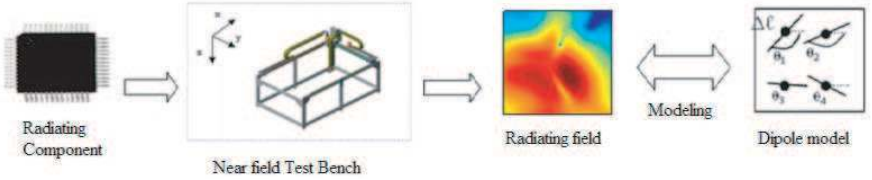

Figure 2. Illustration of the EM NF radiation modeling of electronic devices developed in the IRSEEM laboratory by using an array of elementary dipoles [19].

paper, an examination of metallic wires susceptibility is conducted vis-à-vis the EM radiation in the RF frequency range.

It is worth underlining that the existing works on this EMC radiated susceptibility subject were mainly based either on the radiated far-field interaction on the wires [28–31] or the coupling between EM NF caused by elementary dipoles [32, 33]. But such a case is not sufficiently realistic, for example, for investigating complex electrical system wirings placed in proximity of electronic devices. So, more extended and effective method is required for the analysis of concrete structures.

For the better understanding, this paper is organized in three main sections. Section 2 presents the analytical approaches concerning the hybrid method understudy. It is based on the association of the emission model and also the coupling model induced on the metallic wires by using the analytical formulae established in [28]. Section 3 treats examples of validations with complex forms of metallic wires. In general point of view, two configurations of radiating structures are proposed. The first one is based on a planar microstrip device operating in wideband microwave frequency range. The second one is based on the radiation of a 3D circuit radiating in large band. The last section is the conclusion.

2. DESCRIPTION OF THE WIRING SYSTEM SUSCEPTIBILITY ANALYSIS WITH THE HYBRID METHOD PROPOSED

This hybrid method understudy mainly dedicated to the investigation of electric wire radiated susceptibility is aimed to the determination of the coupling effect on the wire in function of the EM NF perturbations. To realize a complete study, the knowledge of both emission and susceptibility is necessary. This explains the concept of the hybrid

method because the EM field emission can be characterized in different way to the susceptibility analysis.

2.1. Principle of the Radiated Emission Modeling

As described in [19–24], this model developed in the IRSEEM laboratory is based on the determination of the elementary EM dipoles array representing an equivalent radiating source. In other word, the radiated modeling method used is an inverse method calculation with the known radiated EM-data, we use mathematical matrix calculation enabling to find the optimal parameters situated in the horizontal plane of the electronic devices disturbing the wire. The different parameters of dipoles array are the number, geometrical positions and dimensions, space orientations and the excitation currents intensities.

More precisely, this EM radiated model employed [21–23] is based on the array-of-dipole whose detailed mathematical formulations are summarized in the Appendix of this paper. After calculation of the dipole parameters, the electric and magnetic fields at any other height

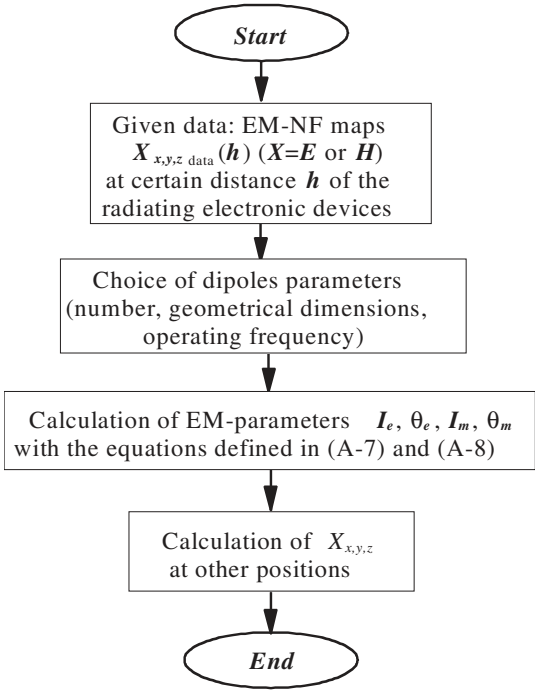

Figure 3. Flow analysis of the radiating emission model used [23].

above the radiating structure can be regenerated. The flow analysis depicted in Fig. 3 summarizes the principle of the radiating modeling employed in this paper.

In the remainder of this paper, we will follow this flow chart to determine the EM-NF radiated by the radiating structure and determine the coupling voltages induced on the metallic wire placed above a metallic ground plane.

2.2. Determination of the Coupling Voltages with the Hybrid Method Proposed

As argued above, this method developed in this paper is realized thanks to the combination of a calculation method enabling to determine the EM fields disturbing the wiring systems independently to the evaluation method of the susceptibility. As illustration, Fig. 4 highlights the global description of the hybrid method proposed in this paper. We can see that it depends on the definition or the geometrical characteristics of the structure to be investigated.

If the calculation of the coupling is made via analytical models,

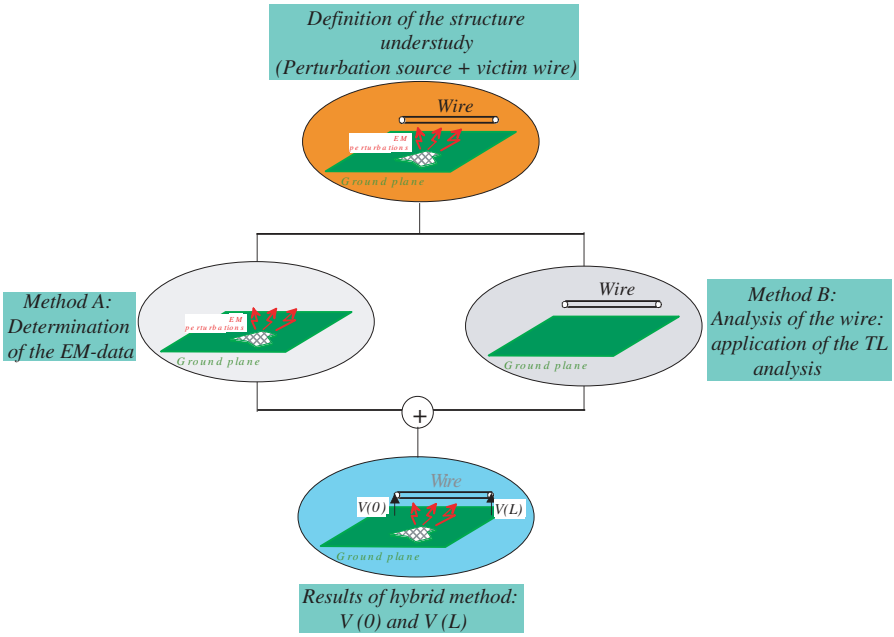

Figure 4. Flow work illustrating the wire susceptibility analysis with the hybrid method understudy.

then the scattered component is not available for the calculation and the total field is considered only with excited field which is incorporated with incident and reflected fields. Thus, the total field in the calculation of fully analytical model is with excited field E and H. Also in this calculation, image theory concept is utilized for ground plane. In the proposed hybrid method, we are considering the cable above the ground plane. In this condition, the scattering field is also included in the calculation of the total field. Finally in the study of the cable susceptibility, we use both the methods to study the coupling mechanism between an electronic component and a TL. We modeled the induced voltage on the line due to electronic component radiation. Then, the analysis is conducted in two parallel steps represented by method A and method B which are described in detail in the next subsections.

2.2.1. Method A: Modeling of the EM Fields Emitted by the Perturbation Circuit

As aforementioned, from any value of given EM data, the hybrid method introduced in this paper enables to analyze the susceptibility of metallic wires victim of EMC effect by expressing the voltage coupling. For that, we use the analytical expressions introduced in [28].

The radiated emission model used in this method consists of the electrical and magnetic dipoles parameters (the orientations θ_e and excitation currents I_e for the electric dipoles and the orientations θ_m and the excitation currents I_m for the magnetic dipoles) knowing the positions and their geometrical dimensions. As reported in [23], we use the expressions of the electric and magnetic fields radiated by an electric dipole (from magnetic vector potential denoted $\vec{A}$) and by a magnetic dipole (from electric vector potential $\vec{F}$). The components (p=$\{x,y,z\}$) of EM fields radiated by an electric dipole can be expressed as:

$$E_{A,p} = f_p\left(k,\, x,\, y,\, z,\, x_0,\, y_0,\, z_0,\, l,\, I_e,\, \theta_e,\, \varepsilon\right), \tag{1}$$

$$H_{A,p} = g_p\left(k,\, x,\, y,\, z,\, x_0,\, y_0,\, z_0,\, l,\, I_e,\, \theta_e\right), \tag{2}$$

and for the magnetic dipole, we have:

$$E_{F,p} = -g_p\left(k,\, x,\, y,\, z,\, x_0,\, y_0,\, z_0,\, l,\, I_m,\, \theta_m\right), \tag{3}$$

$$H_{F,p} = f_p\left(k,\, x,\, y,\, z,\, x_0,\, y_0,\, z_0,\, l,\, I_m,\, \theta_m,\, \mu\right), \tag{4}$$

where f and g are two functions depending on: $(x,\ y,\ z)$ are the coordinates of the point M where electromagnetic field is evaluated, $(x_0,\, y_0,\, z_0)$ are the coordinates of the centre of the dipole, l corresponds to its length, k is the wave number ($2\pi/\lambda$, λ the wavelength), I_e (or

I_m) is the current through the electric (or magnetic) dipole, θ_e (or θ_m) represents the orientation of the electric (or magnetic) dipole in the XY-plane, ε and μ are the permittivity and the permeability of the medium. For N_e electric dipoles and N_m magnetic dipoles, the total EM fields ($X = \{E \text{ or } H\}$) radiated by the dipoles are expressed as:

$$X_p = \sum_{i=1}^{Ne} X_{A,p,i} + \sum_{j=1}^{Nm} X_{F,p,j}, \tag{5}$$

where $p = \{x,\ y,\ z\}$. To determine the unknown parameters of the model, the cartographies of the near-field tangential components E_x, E_y, H_x and H_y (amplitude and phase) are required [23]. This leads then to the matrix system:

$$\begin{pmatrix} [Ex] \\ [Ey] \\ [Hx] \\ [Hy] \end{pmatrix} = \begin{pmatrix} \alpha_{1,1} & \cdots & \alpha_{1,n} \\ \vdots & \ddots & \vdots \\ \alpha_{m,1} & \cdots & \alpha_{m,n} \end{pmatrix} \begin{pmatrix} [I_e \sin(\theta_e)] \\ [I_e \cos(\theta_e)] \\ [I_m \sin(\theta_m)] \\ [I_m \cos(\theta_m)] \end{pmatrix}. \tag{6}$$

where $\alpha_{i,j}$ depend on the frequency, centers and lengths of the dipoles. The least-square inverse method and a division element by element are used to obtain the orientations θ_e and θ_m.

$$[\alpha]^{-1}[E,H] = \begin{pmatrix} [I_e \sin(\theta_e)] \\ [I_e \cos(\theta_e)] \\ [I_m \sin(\theta_m)] \\ [I_m \cos(\theta_m)] \end{pmatrix} = \begin{pmatrix} [A] \\ [B] \\ [C] \\ [D] \end{pmatrix}, \tag{7}$$

$$\theta_e = \text{arctg}\left(\frac{[A]}{[B]}\right) \quad \text{and} \quad \theta_m = \text{arctg}\left(\frac{[C]}{[D]}\right). \tag{8}$$

From where, a matrix $[\beta]$ depending on the space coordinates and the orientations θ_e and θ_m is determined:

$$\begin{pmatrix} [Ex] \\ [Ey] \\ [Hx] \\ [Hy] \end{pmatrix} = \begin{pmatrix} \beta_{1,1} & \cdots & \beta_{1,n} \\ \vdots & \ddots & \vdots \\ \beta_{m,1} & \cdots & \beta_{m,n} \end{pmatrix} \begin{pmatrix} [I_e] \\ [I_m] \end{pmatrix}. \tag{9}$$

2.2.2. Method B: Modeling of the Radiating Susceptibility of the Metallic Wire

Figure 5 illustrates the functioning principle of this model. We consider a metallic wire with length L terminated by $Z(0)$ and $Z(L)$ and aggressed by EM waves presenting electric and magnetic fields above a horizontal ground plane. According to the transmission line (TL) theory, this typically cylindrical cable can be represented by an infinite

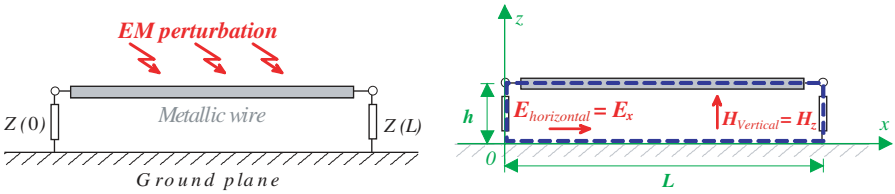

Figure 5. Illustration of the susceptibility model considered.

number of small sections dx, with per unit length parameters as the per unit inductance L_u and the per unit capacitance C_u [33]. Moreover, we recall also that one of the important properties of a transverse EM (TEM) wave on a transmission line is the fact that the EM fields can be related to the propagating voltage and current via the well-known Maxwell's equations. Otherwise, according to the Telegrapher's equations, the voltage $V(y)$ and the current $I(y)$ can be determined with the following linear differential equations:

$$\frac{\partial V(y)}{\partial y} + j\omega \cdot L_u \cdot I(y) = 0, \tag{10}$$

$$\frac{\partial I(y)}{\partial y} + j\omega \cdot C_u \cdot V(y) = 0, \tag{11}$$

where $j = \sqrt{-1}$ and ω is the angular frequency.

The main objective of this study is to calculate the terminal voltages across the wire generated by the EM NF aggression. The field coupling into the wire is considered by the per unit length induced sources V_s and I_s generated by the incident field. The voltage source represents the magnetic coupling generated by normal magnetic field component H_x between the ground plane and the wire:

$$V_s(y) = j\omega \cdot \mu \int_0^h H_x(y, z)dz. \tag{12}$$

where μ is the medium permeability. The electric coupling can be evaluated by the electric field component E_z between the wire and the ground plane. It induces along the surface an accumulation of electric charges representing the per unit length current source:

$$I_s(y) = j\omega \cdot C_u \int_0^h E_z(y, z)dz. \tag{13}$$

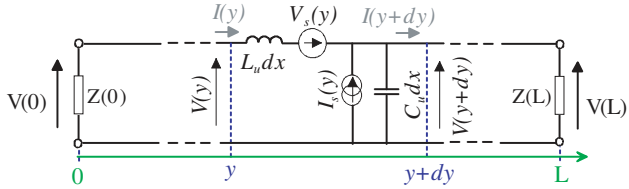

Figure 6. Equivalent circuit of the victim wire including the coupling of an incident field into a transmission line with section dx.

These expressions lead to the representation of the per-unit length equivalent circuit depicted in Fig. 6 with respect to the incident field.

Including the field coupling, the transmission line equations expressed in (10) and (11) are modified by the excitation terms formulated in (12) and (13) as follows:

$$\frac{\partial V(y)}{\partial y} + j\omega \cdot L_u \cdot I(y) = -V_s(y) = -j\omega \cdot \mu \int_0^h H_x(y,z)dz. \tag{14}$$

$$\frac{\partial I(y)}{\partial y} + j\omega \cdot C_u \cdot V(y) = -I_s(y) = -j\omega \cdot C_u \int_0^h E_z(y,z)dz. \tag{15}$$

In the present case, we remain in the context of the quasi-static condition. By taking H_{xa} and E_{za} the average values of the active components of the EM fields in the surface area (having value κ) delimited by the wire and the ground plane, it can be established that Equations (12) and (13) become [32]:

$$V_s.L = -j\omega \cdot \mu \cdot \kappa \cdot H_{xa}, \tag{16}$$

$$I_s = -j\omega \cdot C_u \cdot \kappa \cdot E_{za}. \tag{17}$$

Consequently, due to the EM excitation, the voltages induced over the terminal load $Z(0)$ and $Z(L)$ are written as:

$$V_0 = \frac{Z_0}{Z_0 + Z_L} V_s \cdot L - \frac{Z_0 \cdot Z_L}{Z_0 + Z_L} I_s \cdot L, \tag{18}$$

$$V_L = -\frac{Z_0}{Z_0 + Z_L} V_s \cdot L - \frac{Z_0 \cdot Z_L}{Z_0 + Z_L} I_s \cdot L. \tag{19}$$

For the numerical investigations, the surface formed by the wire and the ground plane is discretized with elementary space steps Δy and Δz. From these parameters, one can express the discrete formula of infinitesimal voltages $V_s(y)$ and currents $I_s(y)$ provided by the

interaction between the EM wave aggressions on the wire given by:

$$V_s(y) = j\omega \cdot \mu \sum_{z=0}^{h} \sum_{y=0}^{d} H_x(y,z)\Delta y \Delta z, \tag{20}$$

$$I_s(y) = j\omega \cdot C_u \sum_{z=0}^{h} \sum_{y=0}^{d} E_z(y,z)\Delta y \Delta z. \tag{21}$$

We point out that this method is limited to the case of the structure operating in the quasi-static condition. In order to verify the effectiveness of the method presented calculations of the coupling voltages across the terminations of wires victim of EM NF perturbations in microwave and low-frequencies are conducted. The next section presents discussions on the results obtained.

3. VALIDATION RESULTS

To confirm the relevance of the hybrid method, metallic wire susceptibility analyses vis-à-vis of the EM NF produced by two different electronic structures were performed. Then, the results obtained are validated with simulations performed with a standard 3D EM full wave solver using the Finite Element Method (FEM). It is important to note that during the analytical computations, the load impedances are $Z(0) = Z(L) = 200\,\Omega$. The metallic wire radius is $r = 0.4\,\text{mm}$. Fig. 7 indicates the geometrical parameters of the metallic wires and its placement above the rectangular metallic planes.

3.1. Susceptibility Analysis with a Planar Electronic Structure Radiating Microwave EM-fields

Figure 8 represents the layout of the microstrip planar circuit considering as the EM NF disturbance source. This circuit resonates at about $f_0 = 0.7\,\text{GHz}$. So, we will check in the following paragraphs

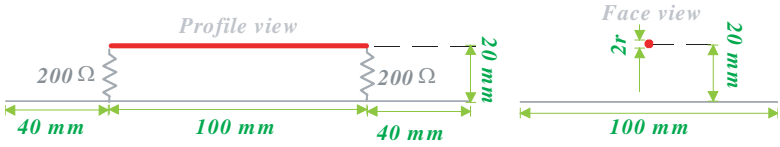

Figure 7. Geometrical description of the metallic wire under test above the ground plane.

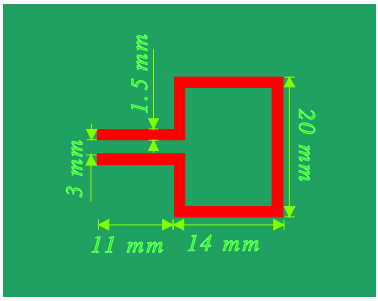

Figure 8. Geometrical description of the radiating circuit.

the influence of the radiations of this loop structure placed in different positions, on wires having some centimeters length.

3.1.1. Configuration A

Figure 9 represents the configurations of a metallic wire associated to a radiating planar rectangular loop above a ground plane designed with HFSS. The planar loop in the XY-plane is placed at 2 mm above the ground plane. The rectangular loop with geometrical dimensions indicated in Fig. 8 was excited by a monochromatic sine wave source with power $P_{in} = 1\,\mathrm{W}$ and having frequency $f_0 = 0.7\,\mathrm{GHz}$.

After application of the radiated modeling method introduced previously in Subsection 2.2.1, we restituted the equivalent source of the disturbing source with the dipole array shown in Fig. 10. These dipoles are of course excited at $f_0 = 0.7\,\mathrm{GHz}$.

We emphasize that the complete dipole model is built from the cartographies of electric and magnetic NFs radiated by the source here the microstrip loop circuit. They have been utilized as reference cartographies. The number and position of the dipoles of the complete model are given by XY coordinates of meshing points. In the present case, the considered complete model contains 1221 electric dipoles and 1221 magnetic dipoles. To reduce the model to insert into HFSS, we defined thresholds on the electric and magnetic currents propagating along the dipoles. Using this reduced model, E and H fields are calculated. This process is done for thresholds to find a tradeoff between the number of dipoles of the reduced model and a good prediction of the fields generated by them in compared with the reference cartographies. The CPU took 2 minutes to build the model. To obtain better results, dipoles of the complete model are placed at the same points as the meshing points (on a XY plane at a different height). It implies that the alpha matrix in (6) must be

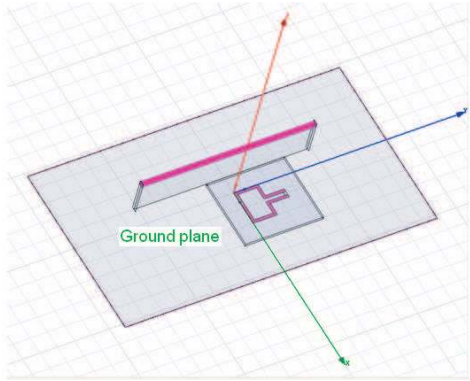

Figure 9. HFSS design of the metallic wire associated to the radiating rectangular planar loop.

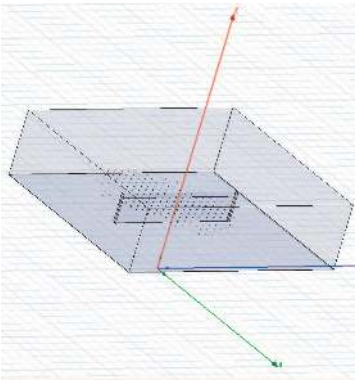

Figure 10. HFSS design of the metallic wire associated with the equivalent radiating source comprised of a set of elementary dipoles.

a square matrix, so its inversion gives better resolution. The used reduced model contains 432 magnetic dipoles and 891 electric dipoles.

Figure 11 present the comparison of the EM-NF simulated from HFSS and modeled with the method introduced in [21–23]. It can be seen that a very good agreement between the behaviors of the EM-NF are found both for the electrical- and magnetic-NF. This explains the validity of the radiated dipole-array model for the configuration understudy.

We have used the electric- and magnetic-NF maps radiated by the array-dipole model to determine the coupling voltage induced at the extremities of the wire for different geometrical positions of the radiating loop $x_p = \{13\,\text{mm}, 14\,\text{mm}, 15\,\text{mm}, 16\,\text{mm}, 17\,\text{mm}\}$ by using the Taylor's method. By reason of symmetry, the voltages at the extremities of the wire determined with the full wave simulation and from the hybrid method developed shown in Table 1 present the same values $V(0) = V(L)$.

We can see that a good correlation between the coupling voltage values $V(0) = V(L)$ is found. As expected, these results illustrate that the coupling effect decreases when the distance between the victim wire and the radiating structure increases. It is worth noting that in addition to the flexibility according to the position the disturbing and the victim structure, the hybrid method developed presents a computation time tens time less than the full wave computation which requires the meshing depending undeniably on the size of the structure and the operating frequency.

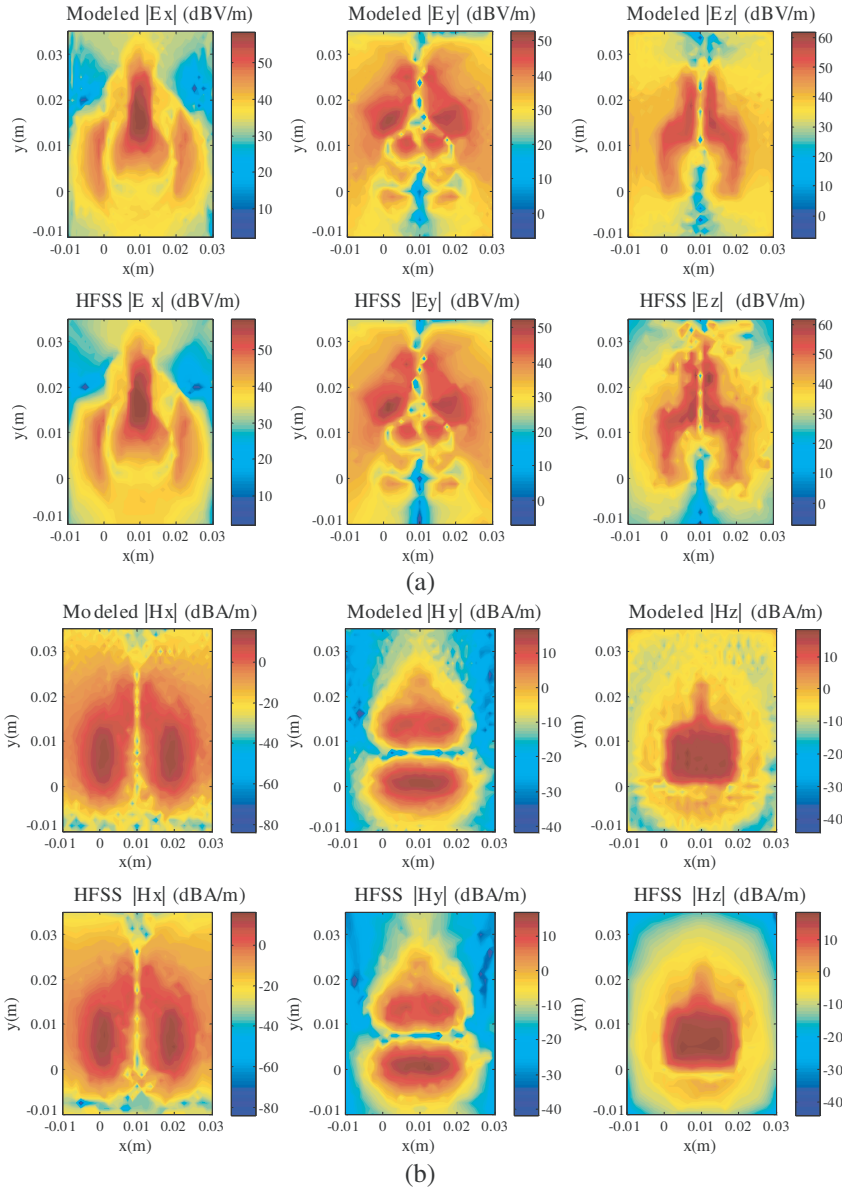

Figure 11. (a) Comparison of electric-NF maps radiated by the loop from HFSS and the modeling with elementary dipoles for $z = 3\,\text{mm}$, $\Delta x = 40\,\text{mm}$ and $\Delta y = 45\,\text{mm}$. (b) Comparison of magnetic-NF maps radiated by the loop from HFSS and the modeling with elementary dipoles for $z = 3\,\text{mm}$, $\Delta x = 40\,\text{mm}$ and $\Delta y = 45\,\text{mm}$.

Table 1. Comparison between the coupling voltages at the extremities of the wires obtained with full wave computation and the hybrid method proposed.

x_p	$V_{HFSS}(0) = V_{HFSS}(L)$	$V_{hybrid}(0) = V_{hybrid}(L)$
13 mm	159 mV	151 mV
14 mm	154 mV	138 mV
15 mm	149 mV	119 mV
16 mm	143 mV	120 mV
17 mm	138 mV	115 mV

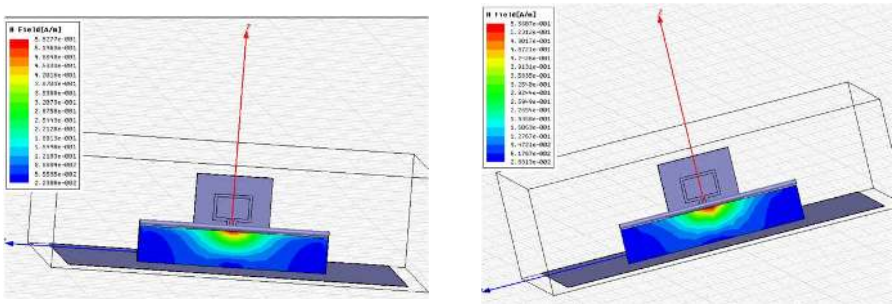

(a) (b)

Figure 12. HFSS design of the metallic wire associated with the disturbing planar circuit placed in the vertical plane parallel to YZ-plane. (a) With load 200 Ω at the termination. (b) With open-ended terminals.

3.1.2. Configuration B

In this case, the radiating microstrip circuit is placed in parallel to the YZ-plane as displayed in Fig. 12. Similar to the previous configuration, this radiating structure was excited by a monochromatic sine wave source having input power $P_{in} = 1$ W and frequency $f_0 = 0.7$ GHz. Then, we analyzed the coupling effect between the wire and the disturbing circuit for the wire loaded by $Z(0) = Z(L) = 200\,\Omega$ and open-ended $Z(0) = Z(L) = \infty$.

Before the applications of the hybrid method based on the Taylor's formulation, we once again compare the maps of the electric-NF and also the magnetic-NF in the YZ-plane positioned at $x = -12$ mm. As results, we generate the maps of the three EM-NF components depicted in Fig. 13. Once again, a good agreement between the

behaviors of the EM-NF is found. With the NF-data radiated by the dipole-array model, we obtained the comparative voltages shown in Table 2(a) and Table 2(b) for $Z(0) = Z(L) = 200\,\Omega$ and open-ended $Z(0) = Z(L) = \infty$ respectively. For these two cases investigated, we can remark that we obtain again voltages representing the coupling effect decreasing with the distance between the disturbing source and victim structure.

In the next steps of this section, we modified considerably the form of the wire by keeping the same physical and geometrical characteristics, in order to consider the complex cases and we checked the relevance of the hybrid method by applying the same analysis as previously. To demonstrate the feasibility of the hybrid method developed, more complicated configurations which are never be investigated before according to the author's best knowledge are considered in the following paragraphs. These configurations are taken into the consideration in view of the realistic automotive applications and its need.

3.1.3. Configuration C

Firstly, we changed the position of the metallic wire above the ground plane as illustrated in Fig. 14(a). As seen in this figure, the wire was

Table 2. (a) Comparison between the coupling voltages at the extremities of the wires obtained with full wave computation and the hybrid method proposed for $Z(0) = Z(L) = 200\,\Omega$. (b) Comparison between the coupling voltages at the extremities of the wires obtained with full wave computation and the hybrid method proposed for $Z(0) = Z(L) = \infty$.

x_p	$V_{HFSS}(0) = V_{HFSS}(L)$	$V_{hybrid}(0) = V_{hybrid}(L)$
14 mm	130 mV	190 mV
16 mm	120 mV	170 mV
17 mm	110 mV	150 mV

(a)

x_p	$V_{HFSS}(0) = V_{HFSS}(L)$	$V_{hybrid}(0) = V_{hybrid}(L)$
14 mm	15 mV	138 mV
16 mm	14 mV	115 mV
17 mm	13 mV	102 mV

(b)

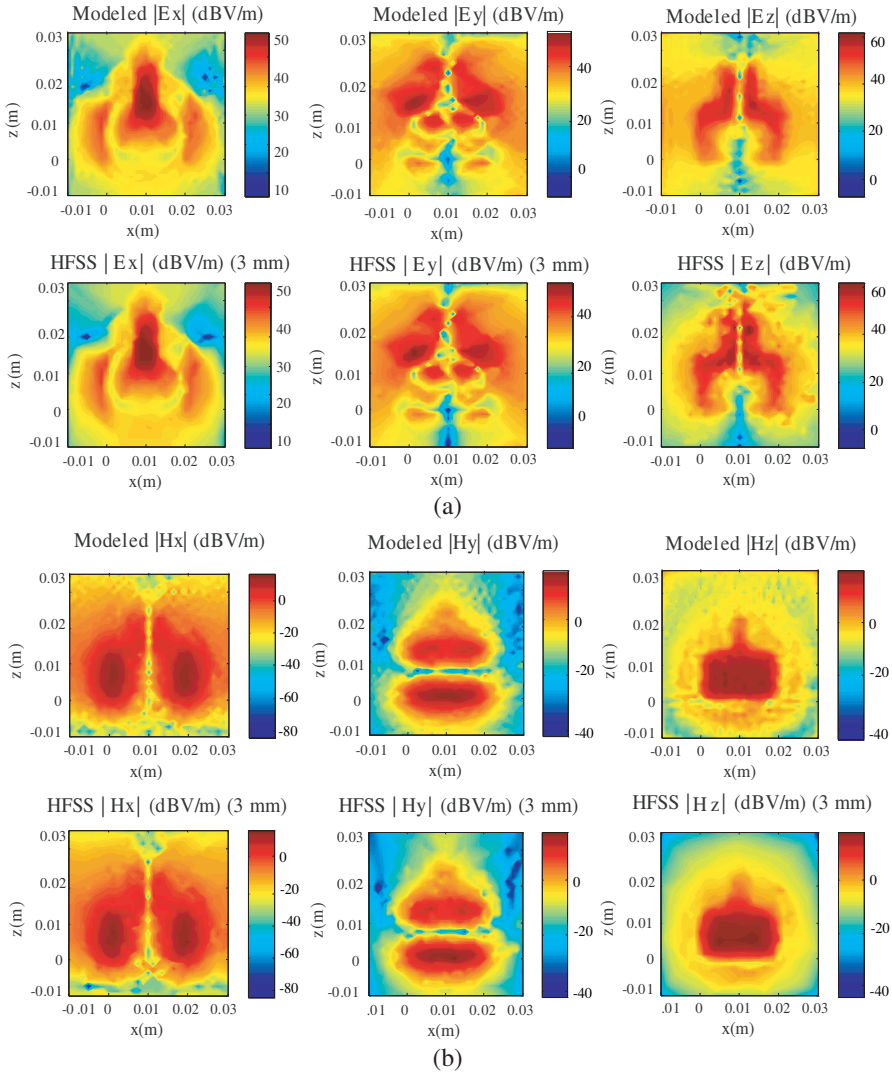

Figure 13. (a) Comparison of electric-NF maps radiated by the disturbing planar circuit from HFSS and the modeling with elementary dipoles for $x = -12\,\text{mm}$, $\Delta y = 40\,\text{mm}$ and $\Delta z = 45\,\text{mm}$. (b) Comparison of magnetic-NF maps radiated by the disturbing planar circuit from HFSS and the modeling with elementary dipoles for $z = 3\,\text{mm}$, $\Delta x = 40\,\text{mm}$ and $\Delta y = 45\,\text{mm}$.

slightly inclined with angle α compared to the ground plane. In this case, we need to determine the horizontal electric-field components and the vertical magnetic-field components within the vertical surface delimited by the ground plane and the wire including the load effects before the calculation of the voltage couplings induced.

To demonstrate the effectiveness of the susceptibility analysis hybrid method understudy, we considered the configuration designed with HFSS depicted in Fig. 14(b). We underline that in this case the length of the wire is still kept equal to 100 mm and the heights of its extremities compared to the reference plane (Oxy) are kept as $h_0 = 20\,\text{mm}$ and $h_L = 25\,\text{mm}$. Here, the terminal loads are $Z(0) = Z(L) = 200\,\Omega$. Similar to the previous tests, we determined the EM-NF radiated by the disturbing radiating source with input sine wave power $P_{in} = 1\,\text{W}$ and with frequency $f_0 = 0.7\,\text{GHz}$. For that various positions of the radiating circuit were considered by changing

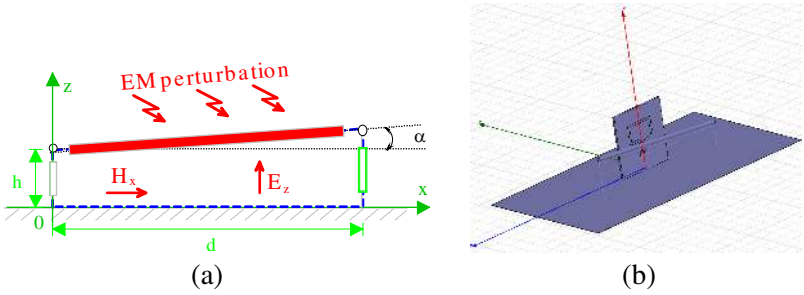

Figure 14. (a) Geometrical illustration of a complex configuration considered with metallic wire inclined above the grounding plane. (b) HFSS design illustrating the configuration considered with victim wire inclined.

Table 3. Comparison between the coupling voltages at the extremities of the wires obtained with full wave computation and the hybrid method proposed for the configuration shown in Fig. 14.

x_p	$V_{HFSS}(0)$	$V_{HFSS}(L)$	$V_{hybrid}(0)$	$V_{hybrid}(L)$
13 mm	204 mV	222 mV	186 mV	249 mV
14 mm	205 mV	232 mV	193 mV	257 mV
15 mm	205 mV	226 mV	215 mV	253 mV
16 mm	204 mV	226 mV	220 mV	250 mV
17 mm	203 mV	230 mV	224 mV	254 mV

$x_p = \{13\,\text{mm}, 14\,\text{mm}, 15\,\text{mm}, 16\,\text{mm}, 17\,\text{mm}\}$ along the x-direction. After application of the hybrid method, we obtain the comparative results shown in Table 3.

3.1.4. Configuration D

To demonstrate the field of validity of the hybrid method understudy, another type of complex configuration was also considered. For that we modified the wire shape as explained in Fig. 15. We recall that in this case the physical characteristic of the wire are kept the same as previously. Whereas the geometrical parameters ($d = 100\,\text{mm}$, $h_0 = 20\,\text{mm}$, $h_L = 30\,\text{mm}$, $\Delta h = 10\,\text{mm}$) are changed as illustrated in Fig. 15(a).

With this structure, we once again proceed with the hybrid method based on the modeling of the NF radiation associated with the analytical method for evaluating the coupling voltages. Therefore,

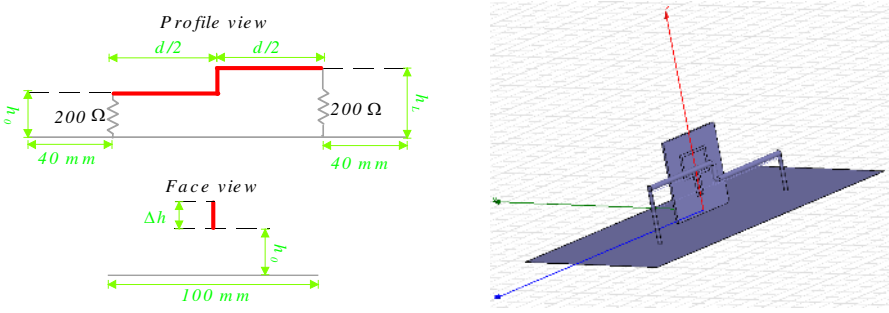

Figure 15. HFSS design illustrating the configuration considered with complex form wire.

Table 4. Comparison between the coupling voltages generated at the extremities of the wires obtained with full wave computation and the hybrid method proposed for the configuration shown in Fig. 15(b).

x_p	$V_{HFSS}(0)$	$V_{HFSS}(L)$	$V_{hybrid}(0)$	$V_{hybrid}(L)$
13 mm	208 mV	220 mV	180 mV	268 mV
14 mm	210 mV	225 mV	181 mV	275 mV
15 mm	214 mV	231 mV	183 mV	283 mV
16 mm	217 mV	237 mV	205 mV	289 mV
17 mm	219 mV	243 mV	223 mV	297 mV

we realize the results established with the hybrid method summed up in Table 4 which are compared with those generated from full-wave simulations. We can see that a good similarity between the two results is found with this case of complex configuration.

3.1.5. Configuration E

In this paragraph, another complicated form of the metallic wire displayed in Fig. 16 is considered. The geometrical parameters of the structure ($d_1 = 47.5\,\text{mm}$, $d_2 = 5\,\text{mm}$, $d_3 = 47.5\,\text{mm}$, $h_0 = 20\,\text{mm}$, $h_L = 30\,\text{mm}$, $\Delta h = 10\,\text{mm}$) are highlighted in Fig. 16(a). During the extraction of the coupling voltages induced at the extremities of the wire, we changed the position of the radiating loop x_p as illustrated in Fig. 16(b).

In this case, we first, calculate the EM-NF in the surface delimited by the wire and the horizontal ground plane. Then, we apply the

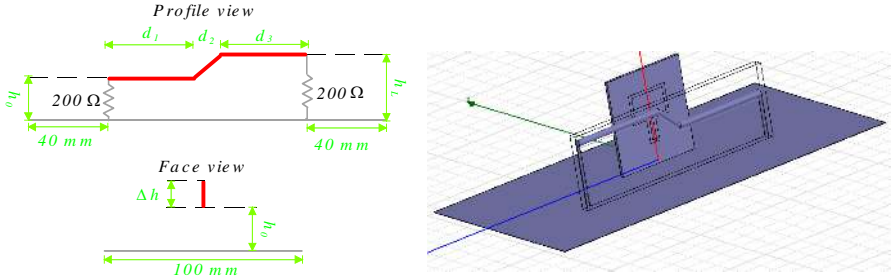

Figure 16. (a) Geometrical description of the configuration considered with complex form wire. (b) HFSS design illustrating the configuration considered with complex form wire associated with the radiating structure.

Table 5. Comparison between the coupling voltages at the extremities of the wires obtained with full wave computation and the hybrid method proposed for the configuration shown in Fig. 16(b).

x_p	$V_{HFSS}(0)$	$V_{HFSS}(L)$	$V_{hybrid}(0)$	$V_{hybrid}(L)$
14 mm	185 mV	185 mV	180 mV	182 mV
15 mm	197 mV	197 mV	196 mV	197 mV
16 mm	213 mV	213 mV	211 mV	212 mV
17 mm	226 mV	226 mV	225 mV	226 mV

coupling voltage formulations at the extremities of the whole wire as previously. Therefore, we recapitulate the results addressed in Table 5. We remark that a good agreement between the two results is obtained. All these results demonstrate the flexibility and the effectiveness of the hybrid method of radiating NF aggression on the metallic wire placed above the ground plane.

3.1.6. Remarks and Discussion

Along the different configurations tested, we observe good agreements between the susceptibility effects on the aggressed metallic wires for any form considered. It is interesting to note that the global advantages of the hybrid method developed in this paper lies on:

- Its flexibility with complex structures either in the side of the EM radiations or the form and the position of the victim wires.
- We emphasize that the present modeling method were run in average computation times of about 10 minutes by using a Matlab program. With the same configuration, by using the default 3D full-wave simulation setting, the HFSS simulations were executed in 1.5 hours.

However, slight differences are found between the results of the coupling voltages and those simulated with HFSS. These numerical differences are mainly due to the spatial resolution or the meshing size assumed during the computation process in the simulation boxes considered which are limited by the power of the computer used. These results can be enhanced by using powerful PC capable to perform calculations with high space resolutions. We underline that the PC employed during the simulations of the structures presented in this paper is equipped a single-core processor XEON 3.4 GHz and 2 GB physical memory with 32-bits Windows XP. Therefore, the size of the data matrix is systematically limited by the physical and virtual memory.

3.2. Validation of the Hybrid Method Proposed with a 3D Radiating Device in Wide Band Frequencies

Because of the unwanted harmonics, the power electronics devices can become disturbing source EM radiations in the electronic circuit boards. For this reason, we propose to investigate the susceptibility of the metallic wire described in Fig. 3 emerged in the EM environment polluted by the radiation of a self coil structure excited by wide frequency band excitation signals.

In this subsection, we considered a radiating device constituted by the self coil described in Fig. 17. This latter is comprised of a self coil structure with core material having permittivity and permeability equal to unity. This radiating device is placed at the proximity of the metallic wire as illustrated by the HFSS design shown in Fig. 17(b). In this case, the terminal loads are equal to $Z(0) = Z(L) = 200\,\Omega$. Fig. 17(b) indicates the geometrical parameters of the whole structure ($a = 25\,\text{mm}$, $b = 9.3\,\text{mm}$, $r = 1.5\,\text{mm}$, $d = 100\,\text{mm}$, $x_p = 19\,\text{mm}$). The different views explain how the radiating device was placed according to the reference axes.

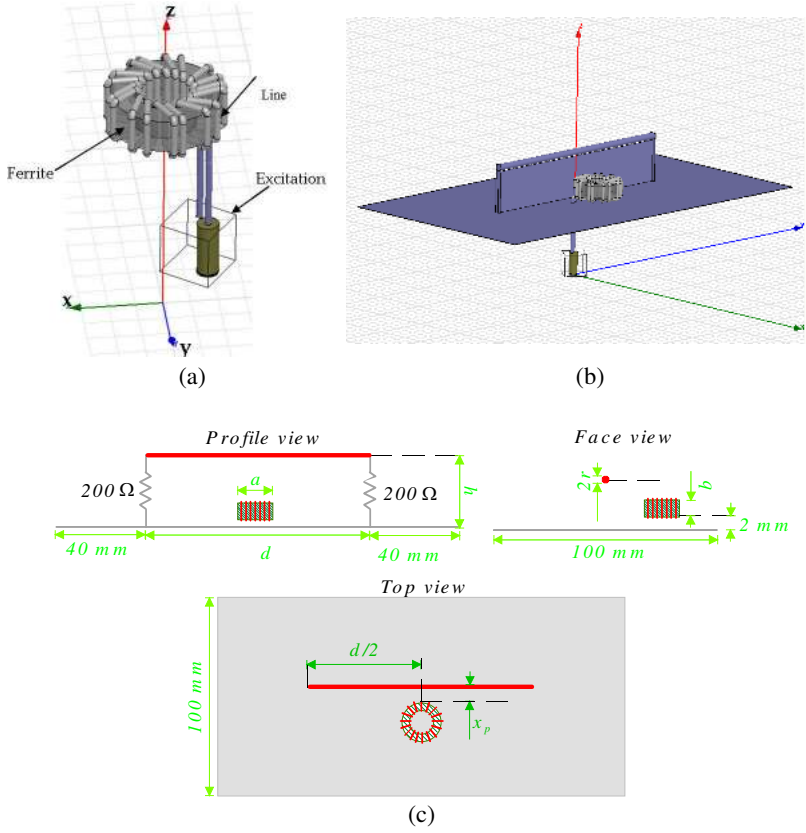

Figure 17. (a) 3D design of the considered radiating circuit. (b) HFSS design of the metallic wire associated a radiating coil self. (c) Geometrical description of the configuration based on the wire associated with a 3D-radiating element formed by a coil self.

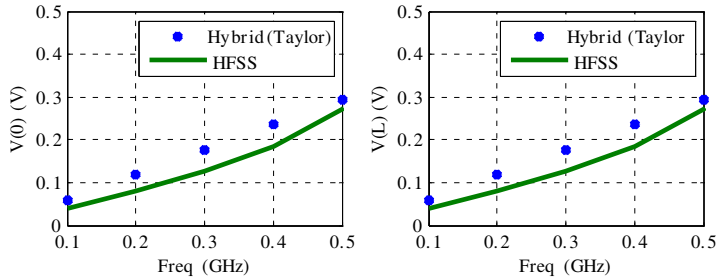

Figure 18. Comparison of coupling voltages induced in the wire of Fig. 4.16(b) calculated with the hybrid method proposed and from HFSS.

By exciting the radiating coil structure with a sine wave signal with power $P_{in} = 1\,\mathrm{W}$ and with frequencies varied from $f_1 = 100\,\mathrm{MHz}$ to $f_2 = 500\,\mathrm{MHz}$, we determine the coupling voltages at the terminations of the wire in the same way as in previous cases with the hybrid method developed. To do this, we first compute the electric-NF horizontal component and the magnetic-NF component of the EM-field radiated in the area delimited by the wire surface and the vertical axis on its extremities. Then, the Taylor's formulations were used to predict the coupling voltages desired.

As results, we obtain the graphs depicted in Fig. 18. It indicates the comparison of full-wave HFSS simulations and the results from the hybrid method. It is note worthy that the hybrid method proposed in this paper offers advantages in terms of the computation time, flexibility with various forms of radiating electronic devices, form of the wiring system above the ground plane and also the position between the source and the victim structure.

4. CONCLUSION

A hybrid method applied to the analysis of complex form metallic wires susceptibility placed in the NF environment radiated by electronic/electrical structures is introduced and investigates. A synthetic methodology based on the combination of the EM-NF radiation model [19–24] and the analytical susceptibility formulation [28] is introduced. It was explained and described how to determine the EM-NF maps from the model based on the use of elementary dipole-arrays developed at the IRSEEM laboratory [19–24]. It is noteworthy that the existing models of wires associated with the ground plane susceptibility are typically based on the totally analytical calculation [31, 32]. These fully analytical methods are only valid if the

radiating source is situated above the wires and not for the case of the radiating source placed below the wire which can be found in most of real applications. Moreover, it is very difficult also to estimate the coupling with fully analytical approach when the perturbation sources are placed close to the cable. In addition, the analytical method introduced in [32] has limitations when the radiating sources are placed very nearer to the victim wire. Hence, this hybrid method allows to overcome the limitations posed by the previous works and the calculation of mean value integration is replaced by the integral calculation of each and every mesh from the centre point of each element of mesh.

To illustrate the relevance of the hybrid method developed in this paper, various complex configurations were considered and validated with full-wave simulations. For that various positions of the radiating structures, for example, constituted by a microstrip planar loop excited by sine wave signals at 0.7 GHz. Then, different complex forms of the metallic wires are also investigated. As results, predictions of coupling effects quantified by voltages induced at the extremities of the wires are realized. Therefore, a good agreement between the full wave simulations was found. Compared to the standard simulations, the method proposed here is advantageous in terms of the flexibility to use for different configurations and also the less computation times. To concretize this advantage, we are currently working on various applications of this hybrid method for the analysis of metallic wires susceptibility with NF radiated by a structure which is difficult to design with standard tools.

But the use of the present hybrid method is less efficient in the context of the far-field perturbations because in this particular case, the analytical method is much simpler and faster. The hybrid method requires a complete model for calculating induced electrical components and it should be capable in NF analysis in all configurations. The methods proposed enables to achieve less computation time in considering the realistic applications. The method proposed in this paper is particularly important for the embedded engines as Automotive/aeronautical applications and also for investigating the integration of high frequency circuits along with cables in close proximity.

In the continuation of this work, we planned to apply this hybrid method for predicting the susceptibility of the wiring structures with metallic grounding implemented in the power electronic systems. The combination of the hybrid method developed here with the plane wave spectrum techniques for the NF treatment introduced in [34–36] is in progress.

ACKNOWLEDGMENT

These research works have been implemented within the frame of the "Time Domain Electromagnetic Characterization and Simulation for EMC" (TECS) project which is part-funded by the Haute-Normandie Region (FRANCE) and the ERDF via the Franco-British Interreg IVA programme No. 4081.

REFERENCES

1. Laurin, J. J., Z. Ouardhiri, and J. Colinas, "Near-field imaging of radiated emission sources on printed-circuit boards," *Proc. of IEEE Int. Symp. EMC*, Vol. 1, 368–373, Aug. 2001.
2. Ostermann, T. and B. Deutschmann, "TEM-cell and surface scan to identify the electromagnetic emission of integrated circuits," *Proc. of 13th ACM Great Lakes Symp. VLSI*, 76–79, Washington DC, USA, 2003.
3. Aunchaleevarapan, K., K. Paithoonwatanakij, W. Khan-ngern, and S. Nitta, "Novel method for predicting PCB configurations for near-field and far-field radiated EMI using a neural network," *IEICE Trans. Commun.*, Vol. E86-B, No. 4, 1364–1376, Apr. 2003.
4. De Daran, F., J. Chollet-Ricard, F. Lafon, and O. Maurice, "Prediction of the field radiated at one meter from PCB's and microprocessors from near EM field cartography," *Proc. of IEEE Int. Symp. EMC*, 479–482, Istanbul, Turkey, May 2003.
5. Archambeault, B., C. Brench, and S. Connor, "Review of printed-circuit-board level EMI/EMC issues and tools," *IEEE Trans. EMC*, 455–461, Vol. 52, No. 2, May 2010.
6. Yang, T., Y. Bayram, and J. L. Volakis, "Hybrid analysis of electromagnetic interference effects on microwave active circuits within cavity enclosures," *IEEE Trans. EMC*, Vol. 52, No. 3, 745–748, Aug. 2010.
7. Vye, D., "EMI by the dashboard light," *Microwave Journal*, Vol. 54, No. 7, 20–23, Jul. 2011.
8. Hubing, T., "Ensuring the electromagnetic compatibility of safety critical automotive systems," Invited Plenary Speaker at the APEMC, Jeju, S. Korea, May 2011.
9. Chen, S., T. W. Nehl, J.-S. Lai, X. Huang, E. Pepa, R. De Doncker, and I. Voss, "Towards EMI prediction of a PM motor drive for automotive applications," *Prof. of 18th Annual IEEE Applied Power Electronics Conference and Exposition*, Vol. 1, 14–22, Orlando, FL, USA, Feb. 9–13, 2003.

10. Wiles, M., "An overview of automotive EMC testing facilities," *Automotive EMC Conference*, Milton Keynes, UK, Nov. 6, 2003.
11. Shin, J., "Automotive EMC standards and testing," Tutorial Workshop Digests on "Introduction to Automotive EMC Testing" at the APEMC, Jeju, S. Korea, May 2011.
12. Liu, K., "An update on automotive EMC testing," *Microwave Journal*, Vol. 54, No. 7, 40–46, Jul. 2011.
13. Revol, B., J. Roudet, J. L. Schanen, and P. Loizelet, "EMI study of a three phase inverter-fed motor drives," *Proc. of the IEEE IAS Annual Meeting*, Vol. 4, 2657–2664, Oct. 3–7, 2004.
14. Benecke, J. and S. Dickmann, "Analytical HF model of a low voltage DC motor armature including parasitic properties," *Proc. of 18th Int. Symp. EMC*, Honolulu, HI, Jul. 9–13, 2007.
15. Mirafzal, B., G. L. Skibinski, R. M. Tallam, D. W. Schlegel, and R. A. Lukaszewski, "Universal induction motor model with low-to-high frequency-response characteristics," *IEEE Trans. Ind. Appl.*, Vol. 43, No. 5, 1233–1246, Sep. 2007.
16. Baudry, D., A. Louis, and B. Mazari, "Characterization of the open ended coaxial probe used for near field measurements in EMC applications," *Progress In Electromagnetics Research*, Vol. 60, 311–333, 2006.
17. Baudry, D., L. Bouchelouk, A. Louis, and B. Mazari, "Near-field test bench for complete characterization of components radiated emission," *Proc. of EMC Compo Conference*, 85–89, Angers, France, Apr. 2004.
18. Baudry, D., F. Bicrel, L. Bouchelouk, A. Louis, B. Mazari, and P. Eudeline, "Near-field techniques for detecting EMI sources," *Proc. of IEEE Int. Symp. on EMC*, Vol. 1, 11–13, Santa Clara, CA, USA, Aug. 2004.
19. Vives-Gilabert, Y., C. Arcambal, A. Louis, F. Daran, P. Eudeline, and B. Mazari, "Modeling magnetic radiations of electronic circuits using near-field scanning method," *IEEE Trans. EMC*, Vol. 49, No. 2, 391–400, May 2007.
20. Vives-Gilabert, Y., C. Arcambal, A. Louis, P. Eudeline, and B. Mazari, "Modeling magnetic emissions combining image processing and an optimization algorithm," *IEEE Trans. EMC*, Vol. 51, No. 4, 909–918, Nov. 2009.
21. Fernandez Lopez, P., A. Ramanujan, Y. Vives Gilabert, C. Arcambal, A. Louis, and B. Mazari, "A radiated emission model compatible to a commercial electromagnetic simulation tool," *Proc. of 20th Int. EMC Zurich Symp.*, 369–372, Zurich,

Switzerland, Jan. 2009.

22. Fernandez-Lopez, P., C. Arcambal, D. Baudry, S. Verdeyme, and B. Mazari, "Radiation modeling and electromagnetic simulation of an active circuit," *Proc. of EMC COMPO*, Toulouse, France, Nov. 17–19, 2009.
23. Fernandez-Lopez, P., C. Arcambal, D. Baudry, S. Verdeyme, and B. Mazari, "Simple electromagnetic modeling procedure: From near-field measurements to commercial electromagnetic simulation tool," *IEEE Trans. Instrum. Meas.*, Vol. 59, No. 12, 3111–3120, Dec. 2010.
24. Ramanujan, A., Z. Riah, A. Louis, and B. Mazari, "Computational optimizations towards an accurate and rapid electromagnetic emission modeling," *Progress In Electromagnetics Research B*, Vol. 27, 365–384, 2011.
25. Chiu, C.-N. and C.-C. Yang, "A solution for increasing immunity against the influence of ground variations on a board integrated GPS antenna", *Progress In Electromagnetics Research C*, Vol. 15, 211–218, 2010.
26. Xie, H., J. Wang, R. Fan, and Y. Liu, "Spice models for radiated and conducted susceptibility analyses of multiconductor shielded cables," *Progress In Electromagnetics Research*, Vol. 103, 241–257, 2010.
27. Paletta, L., J. P. Parmantier, F. Issac, P. Dumas, and J. C. Alliot, "Susceptibility analysis of wiring in a complex system combining a 3-D solver and a transmission-line network simulation," *IEEE Trans. EMC*, Vol. 44, No. 2, 309–317, May 2002.
28. Taylor, C. D., R. S. Sattewhite, and C. W. Harrison, "The response of a terminated two-wire transmission line excited by a nonuniform electromagnetic field," *IEEE Trans. Ant. Prop.*, Vol. 13, No. 6, 987–989, Nov. 1965.
29. Agrawal, A. K. and H. J. Price, "Transient response of multiconductor transmission lines excited by a non uniform electromagnetic field," *IEEE Trans. Ant. Prop.*, Vol. 18, 432–435, Jun. 1980.
30. Rachidi, F., "Formulation of the field to transmission line coupling equations in terms of magnetic excitation field," *IEEE Trans. EMC*, Vol. 35, No. 3, 404–407, Aug. 1993.
31. Atrous, S., D. Baudry, E. Gaboriaud, A. Louis, B. Mazari, and D. Blavette, "Near-field investigation of the radiated susceptibility of printed circuit boards," *Proc. of Int. Symp. on EMC Europe*, Hamburg, Germany, Sep. 8–12, 2008.

32. Leseigneur, C., P. Fernandez-Lopez, C. Arcambal, D. Baudry, and A. Louis, "Near-field coupling model between electronic systems and transmission line," *Proc. of IEEE Int. Symp. EMC*, 22–27, Fort Lauderdale, FL, USA, Jul. 2010.
33. Rajkumar, E. R., A. Ramanujan, M. Bensetti, B. Ravelo, and A. Louis, "Comparison between hybrid methods in the optimization of radiated coupling calculation," *Proc. of 5th ICONIC*, Rouen, France, Nov. 30–Dec. 2, 2011.
34. Ravelo, B., Z. Riah, D. Baudry, and B. Mazari, "E-field extraction from Hx- and Hy- near field values by using plane wave spectrum method," *Eur. Phys. J. Appl. Phys.*, Vol. 53, No. 1, 11201-1–10, Jan. 2011.
35. Ravelo, B., "E-field extraction from H-near-field in time-domain by using PWS method," *Progress In Electromagnetics Research B*, Vol. 25, 171–189, 2010.
36. Ravelo, B., Y. Liu, A. Louis, and A. K. Jastrzebski, "Study of high-frequency electromagnetic transients radiated by electric dipoles in near-field," *IET Microw., Antennas Propag.*, Vol. 5, No. 6, 692–698, Apr. 2011.